Torsional vibrations with bit off bottom: modeling, identification and field data validation

Ulf Jakob F. Aarsnes[a,b,*], Roman J. Shor[c]

[a] *International Research Institute of Stavanger (IRIS), Oslo, Norway*
[b] *DrillWell - Drilling and well centre for improved recovery, Stavanger, Norway*
[c] *University of Calgary, Department of Chemical and Petroleum Engineering, Calgary, Canada*

Abstract

A distributed model of a drill string is presented with Coulomb stiction as a distributed source term to investigate the effect of borehole inclination and borehole friction on the incidence of torsional vibrations along a drill-string. To isolate the effect of this distributed friction, a purely torsional model is first derived and then validated with high frequency field data from two deviated wells from surface and downhole sensors. It is found that by using the behavior of the drill-string during rotational startup, an estimate of both the distributed static friction along the wellbore as well as the relative ratio between static and dynamic friction may obtained. The effects of these two on surface and downhole behavior is presented and then compared with observed behavior in the field.

Contents

1. Introduction

Exploration and production of oil and gas in the deep subsurface, where hydrocarbon reservoirs are found at depths between 2,000 and 20,000 feet, requires that a narrow borehole, between 4 and 24 inches in diameter, be drilled using a slender drill-string through a varied downhole environment and along an often snaking wellpath. Drill string vibrations, and their negative consequences on ROP and equipment, are a well known phenomenon when drilling for hydrocarbons. In particular, the torsional oscillations known as stick slip, which are considered to be the most destructive vibrations, are to be avoided. These stick-slip events are often described as an oscillatory stopping – "sticking" – and releasing – "slipping" – of the bit due to insufficient torque or excessive weight on bit, a behavior which can be observed on the surface through an oscillatory torque pattern in motor torque.

Significant literature exists which seeks to explain the incidence of stick slip through various implementations of bit-rock interaction and various complexities of drill-string dynamic models. The most used models abstract the drill-string as a lumped mass, representing the bottom hole assembly (BHA) inertia, and a torsional spring, representing the drill-string stiffness [1, 2]. Stick-slip is then introduced by making the model unstable through imposing a bit-rock interaction as a *velocity weakening* frictional force (Stribeck-like effect) [3–5], or through the regenerative effect [6–8]. These models may be confounded by introducing higher complexity dynamics at the bit-rock

*Corresponding Author
Email address: ujfa@iris.no (Ulf Jakob F. Aarsnes)

interaction or through higher order models along the drill-string [9–11], but still assume that stick slip is due to the velocity-weakening effect (actual or apparent [8, 12]) of the frictional force at the bit. All these models have been used to demonstrate the occurrence of the limit cycle which exhibits itself as stick-slip and many have been be used to verify various types of stick-slip mitigation controllers, including simple tuned PID controllers [13, 14], impedance matching controllers [15], H-infinity controllers [16, 17], sliding mode controllers [18], and others.

A key factor in common with the above referenced literature is that the bit-rock interaction is used to explain the cause of stick slip. A consequence of this is that the models are unable to explain the occurrence of stick-slip with the bit off bottom (where there is no bit-rock interaction). Off-bottom stick slip is a well known phenomenon from the field, and when mentioned in literature is hypothesized to be caused by a negative difference between static and dynamic *along-string* Coulomb-type friction [19–21]. This is an important phenomena as it indicates that nonlinear frictional forces along the drill-string (and not just the bit rock interaction), in deviated or horizontal wells, plays a significant role in the torsional oscillatory behavior of drill-strings. Models which only incorporate the bit rock interaction as the cause of torsional stick slip fail to explain off-bottom stick slip vibrations which are often observed in field data after connections and in back-reaming operations. This potential cause of stick-slip, as is seen in the off-bottom oscillations, have not received nearly the same analysis or attention in the literature, in particular in the context of occurrence, identification and avoidance.

The effect of the distributed, along-string, Coulomb friction, becomes an increasingly prominent feature of torsional drill string dynamics in wellbores with high-inclination laterals. The nonlinear nature of the Coulomb friction can excite a wide range of frequencies where higher order modes become essential for representing the dynamics of the system, in particular for long wells. Hence, lumped approximations of the drill string easily fall short, and it is desirable to develop a distributed model representation of the torsional dynamics, along the lines of [22, 23]. Specifically, a distributed model where also the distributed nature of the Coulomb friction is represented.

1.1. Contribution and approach

The approach taken in the present work is to use a distributed model of the drill string with the Coulomb friction given as a distributed source term implemented as a inclusion. The distributed nature of the model enables it to capture the full range of possible dynamics regardless of well length and survey. At the same time, the relative mathematical simplicity of the formulation, a 1-D wave equation with a source term, enables us to derive simple yet accurate relations for the expected period, amplitude and behavior of the stick-slip limit cycle. These relations can in turn be used to estimate dynamic and static friction

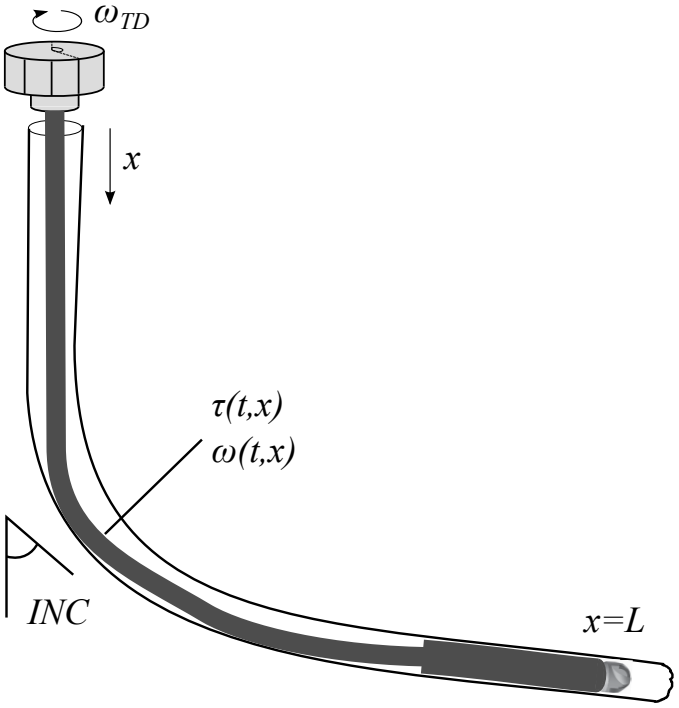

Figure 1: Schematic indicating the distributed drill string lying in deviate borehole.

factor which have important applications for directional drilling [24, 25].

To validate the model we compare the response of the model to field data from rotational startups, off bottom and without any axial movement, after a connection. This allows us to *isolate* the effect of the angular motion of the drill string against *only* the Coulomb friction of the well bore. That is, without any bit rock interaction or coupling with the axial dynamics.

A significant attraction with this approach is that, having isolated the effect of the torsional Coulomb friction in this way, it can be quantified in a rigorous manner, and then in a future work combining with axial motion and existing results on bit-rock interaction, for simulating the full on-bottom dynamics.

2. Model

2.1. Torsional dynamics of drill string

We use a distributed model, similar to [22, 23, 26], except that in this case we consider only the torsional dynamics. That is, for the angular motion, we denote the angular velocity and torque as $\omega(t,x), \tau(t,x)$, respectively, with $(t,x) \in [0,\infty)\times[0,L]$. The torque is found from shear strain, given as twist per unit length, and letting ϕ denote the angular displacement in the string s.t. $\frac{\partial\phi(t,x)}{\partial t} = \omega(t,x)$, we have $\tau(t,x) = JG\big(\phi(t,x) - \phi(t,x+dx)\big)/dx$. Here J is the polar moment for inertia and G is the shear modulus. Hence the equations for the angular motion are

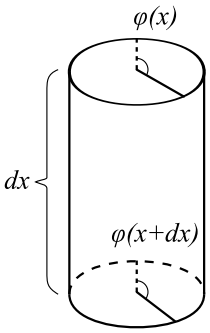

Figure 2: Infinitesmal drill string element.

given by

$$\frac{\partial \tau(t,x)}{\partial t} + JG\frac{\partial \omega(t,x)}{\partial x} = 0 \tag{1}$$

$$J\rho\frac{\partial \omega(t,x)}{\partial t} + \frac{\partial \tau(t,x)}{\partial x} = S(\omega,x), \tag{2}$$

where the source term is due to frictional contact with the borehole and is modeled as

$$S(\omega,x) = -k_t\rho J\omega(t,x) - \mathcal{F}(\omega,x), \tag{3}$$

where k_t is a damping constant representing the viscous shear stresses between the pipe and drilling mud, and $\mathcal{F}(\omega)$ is a differential inclusion, to be described, representing the Coulomb friction between the drill string and the borehole.

2.2. Discontinuities of multiple sectioned drill string

The lowermost section of the drill string is typically made up of drill collars which may have a great impact on the drill string dynamic due to their added inertia. In particular, the transition from the pipes to collars in the drill string will cause reflections in the traveling waves due to the change in characteristic line impedance [22].

We split the drill string into a pipe section with polar moment of inertia and lengths J_p, L_p and a collar section with the same parameters given as J_c, L_c. We use τ^+, ω^+ to denote the strain and velocity at the top of the drill collar and τ^-, ω^- at the bottom of the pipe, see Fig. 3. Enforcing the boundary conditions $\omega^+ = \omega^-$ and $\tau^+ = \tau^-$ at the transition.

2.3. Coulomb friction as an inclusion

The Coulomb friction is modeled as an inclusion

$$\begin{cases} \mathcal{F}(\omega,x) = F_c(x) f_{rat}, & \omega > \omega_c, \\ \mathcal{F}(\omega,x) \in [-F_c(x), F_c(x)], & |\omega| < \omega_c, , \\ \mathcal{F}(\omega,x) = -F_c(x) f_{rat}, & \omega < \omega_c, \end{cases} \tag{4}$$

where $\omega_{threshold}$ is the threshold on the angular velocity where the Coulomb friction transitions from static to dynamic, $f_{rat} \in [0,1]$ is the the ratio between the static and

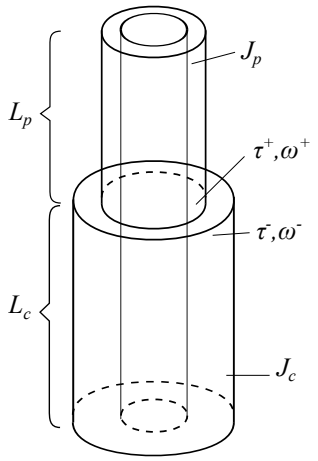

Figure 3: Collar-Pipe transition.

dynamics Coulomb friction, and $\mathcal{F}(\omega) \in [-F_c, F_c]$ denotes the inclusion where

$$\mathcal{F}(\omega,x) = -\frac{\partial \tau(t,x)}{\partial x} - k_t\rho J\omega(t,x) \in [-F_c(x), F_c(x)], \tag{5}$$

and take the boundary values $\pm F_c(x)$ if this relation does not hold.

To obtain the maximum Coulomb torque function $F_c(x)$, we employ the classic Coulomb friction law, which states that the friction opposing a motion horizontal to the plane is proportional to the normal force with the coefficient μ [19]. Thus we obtain

$$F_c(x) = \mu \sin(\text{INC})\rho g A(x) r_o(x), \tag{6}$$

where INC is the wellbore inclination, g is the acceleration of gravity, $A(x)$ is the cross sectional area of the drill string, $r_o(x)$ is the outer radius of the drill string. The friction factor μ is dependent on the wellbore roughness, mud properties, etc.

Note that the relation (6) is simplistic in that the normal force is affected by other effects than just gravity, with tortuosity being a particular important parameter [27]. Consequently, to compensate for such un-modeled effects, the friction factor μ can be tuned (typically increased). For the case studied in [28], tortuosity was found to increase torque progressively with MD with a 28% increase reported at 17,000 ft when drilled with a RSS with an unwanted Dog Leg Severity of 0.45 and 0.41 deg/100ft in the curve section and the slant section, respectively.

2.4. Boundary condition

At the topside boundary, the Top Drive is actuated by a motor torque τ_m controlled by a PI controller to a desired velocity set-point ω_{SP}:

$$e = \omega_{SP} - \omega_{TD} \tag{7}$$

$$I_e = \int_0^t e(\xi)\mathrm{d}\xi \tag{8}$$

$$\tau_m = k_p e + k_i I_e, \tag{9}$$

with a proportional gain of $k_p = 38$ kNm per m/s and an integral gain of $k_i = 100$ kNm per m/s^2.

The topdrive has the inertia I_{TD} and hence satisfies the dynamics

$$\frac{\partial \omega_{TD}}{\partial t} = \frac{1}{I_{TD}}\Big(\tau_m - \tau_0\Big), \tag{10}$$

and finally, the angular velocity at the top of the drill string is given as $\omega_0 = \omega_{TD}$.

3. Numerical implementation

3.1. Overview

In the numerical implementation of the model the wave equation (1),(2) is transformed into their Riemann invariants the resulting transport equations of the system is then solved with a first order upwind scheme [29]. The first order upwind scheme is used to ensure high numerical robustness and to avoid spurious oscillations, as it was found that higher order schemes performed poorly due to the temporal discontinuities introduced by the distributed differential inclusions which are used to represent the Coloumb friction. Numerical accuracy can then be ensured by having a sufficiently fine spatial grid, and this is an amenable approach due to the fact that simulation speed is not of critical importance for the present study.

In all simulations a spatial grid of 500 cells was used for the drill string and the time-step was chosen so as to enforce the CFL condition.

3.2. Derivation of Riemann invariants

Define the Riemann invariants

$$\alpha = \omega + \frac{c_t}{JG}\tau, \quad \beta = \omega - \frac{c_t}{JG}\tau, \tag{11}$$

where $c_t = \sqrt{\frac{p}{J}}$ is the velocity of the torsional wave. The variables α, β satisfies the diagonalized PDE system

$$\frac{\partial \alpha}{\partial t} + c_t \frac{\partial \alpha}{\partial x} = -\mathcal{S} \tag{12}$$

$$\frac{\partial \beta}{\partial t} - c_t \frac{\partial \beta}{\partial x} = -\mathcal{S}. \tag{13}$$

with the source term

$$\mathcal{S} = \frac{S}{J\rho} = k_t(\alpha + \beta) + \frac{1}{J\rho}\mathcal{F}. \tag{14}$$

3.3. Discontinuities of a multi-section drill string

At a discontinuity in the drill string impedance $\frac{c_t}{JG}$, we have to enforce

$$\omega^+ = \omega^-, \qquad \tau^+ = \tau^-, \tag{15}$$

which entails

$$\beta^+ = \frac{1}{1+\bar{Z}}\big(\alpha^+(1-\bar{Z}) + 2\bar{Z}\beta^-\big) \tag{16}$$

$$\alpha^- = \frac{1}{1+\bar{Z}}\big(2\alpha^+ - (1-\bar{Z})\beta^-\big) \tag{17}$$

where we have denoted the relative magnitude of the impedance as

$$\bar{Z} = \left[\frac{c_t}{JG}\right]^- \Big/ \left[\frac{c_t}{JG}\right]^+. \tag{18}$$

We note that for the case of the same material being used at both sides of the discontinuity, the only change is in the polar moment of inertia. That is, for a pipe-collar sections of e.g. steel, we have, following Fig. 3

$$\bar{Z} = \frac{J_c}{J_p}. \tag{19}$$

Note the meaning of (16)–(17) as reflections of incoming waves from both sides, as they are split into an upward and a downward traveling wave.

3.4. Upwind scheme

In the numerical treatment of the model, $\mathcal{F}$ is implemented as follows. For cell size Δx and and time step Δt, and at cell # j and time step # k

$$\tilde{\mathcal{F}}_j^k = \frac{1}{2\Delta t}\Bigg(\alpha_j - c_t\frac{\Delta t}{\Delta x}(\alpha_j - \alpha_{j-1}) + \tag{20}$$

$$\beta_j + c_t\frac{\Delta t}{\Delta x}(\beta_{j+1} - \beta_j) + \Delta t k_t(\alpha_j^k + \beta_j^k)\Bigg), \tag{21}$$

and limited by

$$\mathcal{F}_j^k = \begin{cases} \operatorname{sgn}(\tilde{\mathcal{F}}_j^k)\min(|\tilde{\mathcal{F}}_j^k|, F_c), & \frac{|\alpha_j^k + \beta_j^k|}{2} \le \omega_c \\ \operatorname{sgn}(\tilde{\mathcal{F}}_j^k)\min(|\tilde{\mathcal{F}}_j^k|, f_{rat}F_c), & \frac{|\alpha_j^k + \beta_j^k|}{2} > \omega_c \end{cases} \tag{22}$$

The model is updated with an upwind scheme according to

$$\alpha_j^{k+1} = \alpha_j^k - c_t\frac{\Delta t}{\Delta x}(\alpha_j^k - \alpha_{j-1}^k) - \Delta t k_t(\alpha_j^k + \beta_j^k) - \mathcal{F}_j^k \tag{23}$$

$$\beta_j^{k+1} = \beta_j^k - c_t\frac{\Delta t}{\Delta x}(\beta_j^k - \beta_{j+1}^k) - \Delta t k_t(\alpha_j^k + \beta_j^k) - \mathcal{F}_j^k. \tag{24}$$

4. Preliminary model analysis

In this section we will perform a preliminary model analysis on a synthetic well example with a simple trajectory in an effort to extract some general characteristics of the model dynamics. We consider in the following a well, **Well A**, with a 1000 meter long 60 degree lateral section as sketched in Fig. 4.

4.1. Stick slip cycle description

The trend of a typical drill string rotation startup is shown in Fig. 5, with the result of the drill string entering into a stick slip cycle.

The torque and velocity profiles showing a single period of this cycle is shown in Fig. 7–6. The stick slip cycle is described in the following:

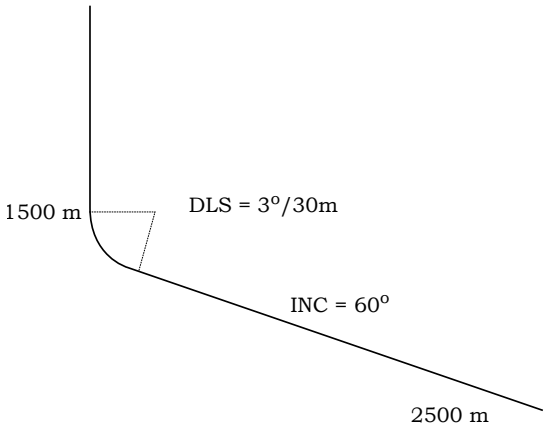

Figure 4: Wellbore survey for **Well A**, used in the synthetic case.

22s: The lower section of the drill string is stationary, kept in place by the Coulomb stiction.

27s: Rotation of the top drive is twisting the drill string, adding torque to the system.

31s: The break-off torque of the system is almost reached, overcoming the Coulomb stiction.

32s: Coulomb stiction has yielded causing the stored torque to violently accelerate the lower, previously station, section of the drill string.

33s: The angular velocity of the drill string is negatively reflected at the stiff top-drive, causing potential negative velocities.

34s: The negative reflection forces the drill into being stationary, where it is *caught* by Coulomb stiction, starting next period of the cycle.

4.1.1. Break-off torque and twist

The point in time where the bottom of the BHA yields from the Coulomb friction and starts to mobilize corresponds to the point when the rotational work done is sufficient to overcome the total Torque imposed by the distributed Coulomb friction.

To find this value, the required energy to release the BHA, consider the family of steady state solutions of (1)–(2) for $\omega(x=0)=0$:

$$\frac{\partial \tau}{\partial x} = -\mathcal{F}(x), \tag{25}$$

where we recall that the Coulomb friction is modeled as the inclusion $\mathcal{F}(x) \in [-F_c, F_c]$. That is, using the boundary condition $\tau(x=L)=0$, as the bit is off bottom, we have that the maximum possible value for torque at steady-state, denoted $\overline{\tau}(x)$, is given as

$$\overline{\tau}(x) = \int_L^x -F_c(\xi)\mathrm{d}\xi. \tag{26}$$

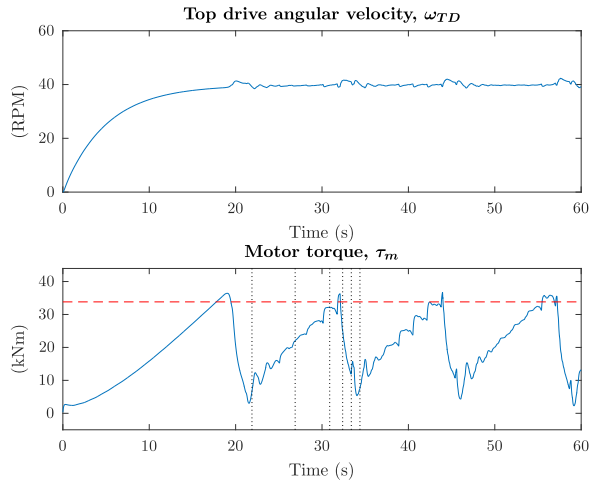

Figure 5: Trend showing the applied torque and top drive angular velocity for a off-bottom startup entering a stick slip for **Well A**.

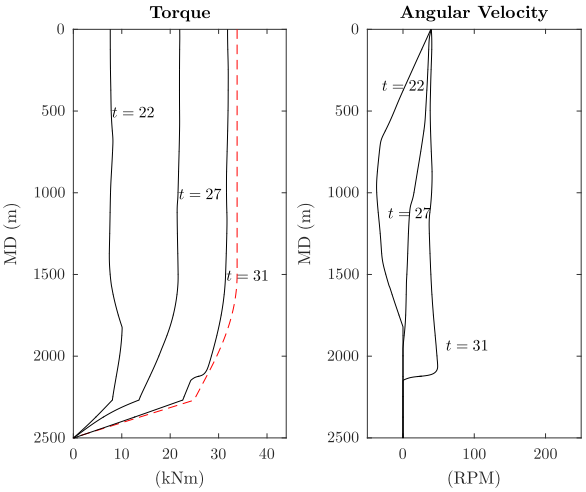

Figure 6: Profile snapshots in time showing the sawtooth pseudo limit-cycle buildup for **Well A**, with the trends shown in Fig. 5. The break-off torque profile is shown as a red dotted line.

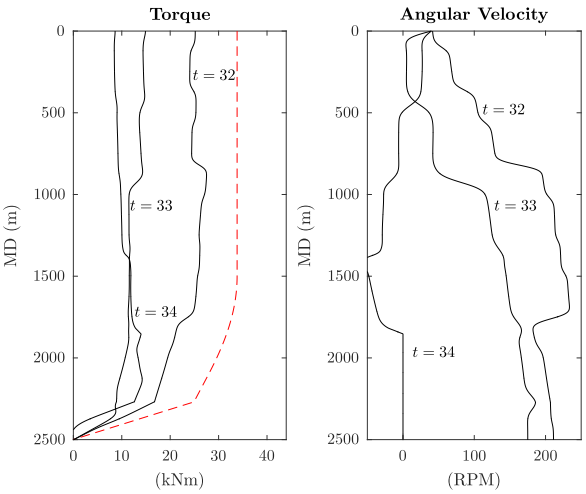

Figure 7: Profile snapshots in time showing the sawtooth pseudo limit-cycle release, for **Well A**, with the trends shown in Fig. 5. The break-off torque profile is shown as a red dotted line.

The maximum torque is encountered at the top-drive

$$\overline{\tau}_m = \int_L^0 -F_c(x)\mathrm{d}x. \tag{27}$$

Next, noting the relation for torque from strain, where we without loss of generality can assume $\phi(x=0)=0$,

$$\tau = JG\frac{\partial \phi}{\partial x}, \tag{28}$$

we find the corresponding angular displacement as

$$\phi(x) = \int_0^x \frac{\tau(\xi)}{J(\xi)G(\xi)}\mathrm{d}\xi. \tag{29}$$

4.1.2. Amplitude of oscillations

The magnitude of the released torque is given as the difference between the static and dynamic friction, that is, by the coefficient $1-f_{rat}$. Due to the negative velocity reflection at the top-drive however, the amplitude of the torque oscillations, given the minimum value of the torque, is better approximated by by twice this value. That is, over a typical limit cycle, with a period spanning the set t_p, the minimum motor torque seen at a stiff top-drive, denoted by $\underline{\tau}$, is approximated by

$$\min_{t\in t_p} \tau(x) \equiv \underline{\tau}(x) \approx \overline{\tau}(x)(1-2(1-f_{rat})). \tag{30}$$

This means that we could expect the motor torques, τ_m, to have minima below zero, during a stick slip period, when $f_{rat} < 0.5$.

4.2. Period of oscillations

To find the period of the oscillations, we first find the amount of drill string twist which corresponds to the change in torque between the bottom and top of a stick slip cycle.

Recall that we approximated the change in torque as

$$\begin{aligned}\overline{\tau}(x) - \underline{\tau}(x) &= \overline{\tau}(x) - \overline{\tau}(x)\big(1-2(1-f_{rat})\big) &(31)\\ &= \overline{\tau}(x)2(1-f_{rat}). &(32)\end{aligned}$$

The resulting change in twist can be obtained from recalling (28) to obtain

$$\Delta\phi(x) = 2(1-f_{rat})\int_0^x \frac{\overline{\tau}(x)}{J(\xi)G(\xi)}\mathrm{d}\xi. \tag{33}$$

We are interested in the required change in twist at the top-drive, $\Delta\phi(0)$, which enables us to find the build-up time of the cycle as

$$t_{bu} = \frac{\Delta\phi(0)}{\omega_{TD}}. \tag{34}$$

When the drill string is free, i.e. there is no build up time, the drill string oscillation will be dominated by the fundamental period of the free drill string, which is dependent on the drill pipe and collar length and the relative

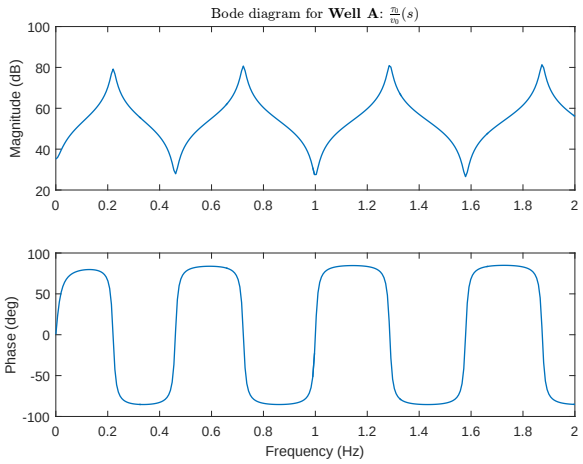

Figure 8: Bode diagram of the free torsional dynamics of the drill string. The first fundamental resonant mode, corresponding to the fundamental period, can be seen to be located at 0.22 Hz, corresponding to a period, t_{fp}, of 4.5 seconds.

impedance $\bar{Z}$ [26]. Similarly, as the drill string breaks free, the trajectory will follow close to one fundamental period before getting stuck again. That is, denoting the fundamental period of the drill string as t_{fp}, see Fig. 8, the period of the limit cycle is

$$t_p = t_{bu} + t_{fp}. \tag{35}$$

This allows us to heuristically distinguish between two different types of oscillations:

1. The oscillation is dominate by the fundamental period of the drill string. The torque trend resembles that of free oscillations.

2. The oscillation is dominated by the torque build up. A characteristic sawtooth pattern of the torque is obtained.

These two types of stick slip oscillations can be distinguished from the two respective time constants contributing to the total period:

$$\textbf{Inertia dominated: } t_{bu} < t_{fp}, \tag{36}$$
$$\textbf{Stick dominated: } t_{bu} > t_{fp}. \tag{37}$$

(36)–(37) does not denote a sharp distinction, but rather a rough guideline as to what kind of behavior to expect.

Also note that the previous derivation assumes the drill-string reaches the maximum torque profile $\overline{\tau}(x)$ and swings all the way back to $\underline{\tau}(x)$. In practice, shocks and torque perturbations will typically cause the drill string to break loose before the maximum steady-state torque profile is reached and viscous dissipation will prevent the drill string from swinging all the way back. Hence, actual observed period of oscillations will be slightly lower than this approximation.

4.3. Analysis summary

The findings of the preliminary model analysis performed in this section can be summarized as follows

- Break-off torque, proportional to friction factor μ:

$$\overline{\tau}_m = \int_L^0 -F_c(x)\mathrm{d}x. \tag{38}$$

- Amplitude of oscillations, proportional to absolute difference between static and dynamic friction factor:

$$\Delta\tau_m \approx \overline{\tau}_m 2(1-f_{rat}). \tag{39}$$

- Period of oscillations, t_p, sum of the time to reach build up torque, $t_{bu} = \frac{\Delta\phi(0)}{\omega_{TD}}$, and the fundamental period of the drill string, t_{fp}:

$$t_p \approx \frac{\Delta\phi(0)}{\omega_{TD}} + t_{fp}. \tag{40}$$

4.4. Synthetic simulations

The conclusions summarized in Section 4.3 is illustrated with simulations performed on **Well A** which are shown in Figures 9, 10 and 11.

In modeling the Coulomb friction the two key parameters to be specified is the static friction factor μ and the static to dynamic friction ratio f_{rat}. The individual effect of these two parameters are shown in Fig. 9 and Fig. 10 respectively. In particular we note how the break off torque increases with the friction factor μ in Fig. 9, and how the amplitude of the oscillations increases with smaller f_{rat} in Fig. 10. Finally, note how both these two parameters, in addition to the RPM, all play a role in deciding the period of the oscillations.

5. Model comparison with field data

To validate the modeling approach taken in the present work, a simulation study was undertaken to compare the behavior of the model to that of recorded field data. The data was collected from a total of 46 torsional start-ups (after a connection had been performed) for two different wells, and for well depths ranging from 1589 meters to 2953 meters. The main findings of this study is presented in the following.

5.1. Simulation study case description

Field data for two deviated wells, the surveys of which are shown in Figures 12a and 12b, are used to validate the model. Rotational data – rotary rpm and torque – is recorded at 100 Hz and provides a clear picture of both the rpm set-points used during the drilling process and the torsional drill-string response. Since the torque is recorded via current integration within the variable frequency drive (VFD), it includes the effects of inertia of the top drive

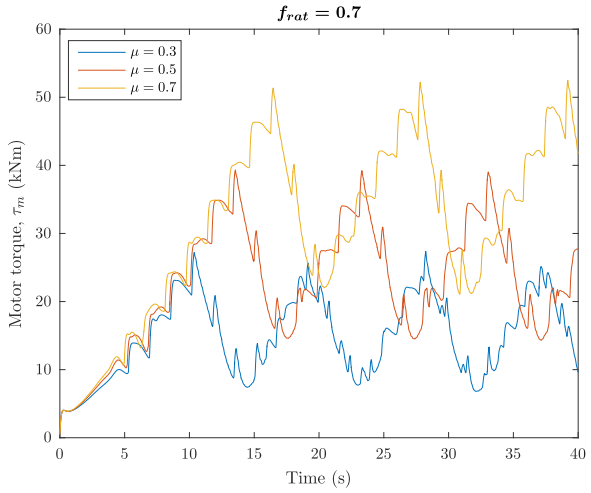

Figure 9: Effect of changing the friction factor μ. Simulations shown for **Well A**, and a set-point of $\omega_{SP} = 60$RPM.

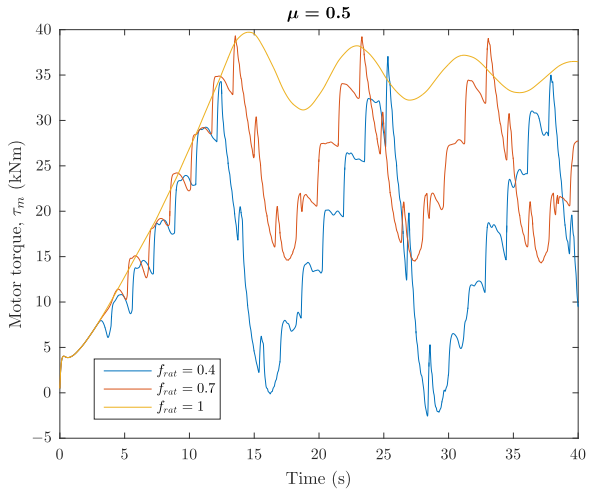

Figure 10: Effect of changing the ratio in the Coulomb friction f_{rat}. Simulations shown for **Well A**, and a set-point of $\omega_{SP} = 60$RPM. Note the bifurcation happening beetween $f_{rat} = 0.7$ and $f_{rat} = 1$, making the system stable, causing the oscilliations to die out.

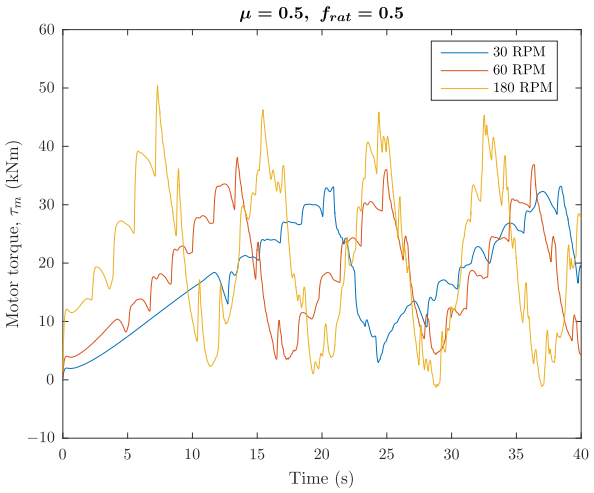

Figure 11: Effect of changing the RPM. Simulations shown for **Well A**. Higher RPM results in shorter periods of the oscillations as the break-off torque is built faster.

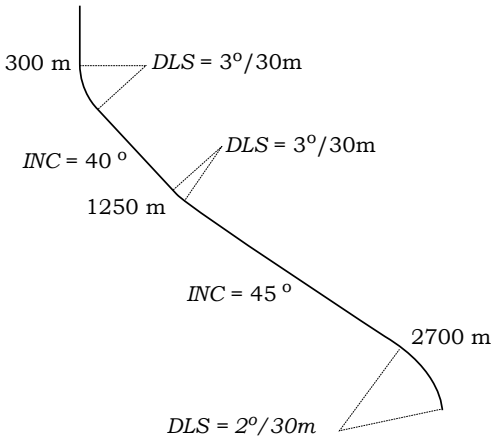

(a) **Well B**

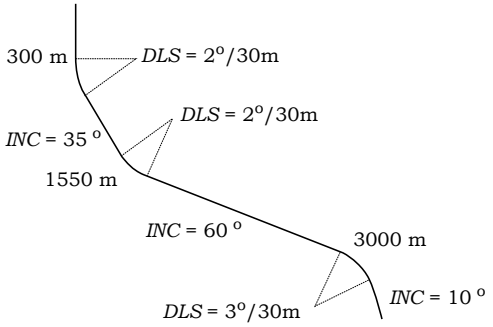

(b) **Well C**

Figure 12: Wellbore surveys of the two field wells

motor, which is known for the frequency band of interest and is accounted for in the model (see Eq. 10). In all cases presented herein, the drill-string starts at rest with zero torque at the surface. However, the stored torsional energy within the drill-string is not known. In both cases, the drill-string design is a simple directional assembly which is simplified to a 230 meter $5^3/_4$" OD BHA and monodiameter drillpipe to the surface. Downhole rpm and vibration data was collected for drilling performance improvement and control system verification and included continuous low frequency (0.5Hz) data as well as occasional burst sequences of high frequency data (125 Hz). For Well B, downhole data was sampled continuously at 125 Hz and then processed to record minimum, maximum and mean rpm for the 0.5 second sampling window.

A phase shifting phenomena is noted in both the surface and downhole data which occurs in conjunction with axial motion of the drill-string and any subsequent changes in weight on bit. A phase shift from surface oscillation to downhole oscillations is visible when the bit touches bottom (indicated by positive weight on bit) which causes a temporary reduction in downhole oscillation frequency as additional energy is stored in the drill-string to counter the now non-zero torque on bit. A similar phase shift is noted on surface in the torque signal once this torque wave reaches surface.

5.2. Parameter fitting

The results of a parameter sensitivity study are shown in Figures 13a and 14a where the color axis corresponds to the L_2-norm of the error between the model fit and the recorded surface torque for the first cycle and a half of the torque oscillation in the first subfigures and for the two subsequent cycles in the second subfigures. This ensures a match with the peak torque, the drop-off torque and the subsequent release torque.

These two sets of figures show that a functional relationship between μ and f_{Rat} gives the minimal error over a range of $\omega_{threhold}$ values. Therefore, it is also necessary to evaluate the model fit during steady-state torsional oscillation but before the drilling state changes – i.e. a change in axial tension or a change in the bit boundary condition. Therefore, a second set of optimizations are conducted, the results of which are shown in figures 13b and 14b.

5.3. Well B: Inertia dominated oscillations

Recorded field data and a model fit for two different depths, 1,733 m and 2,235 m are shown in Figures 15 and 16. In each figure, the top plot shows the surface (in red) and downhole (dashed) recorded data as well as the modeled data (in blue and yellow, respectively). The bottom plot shows surface torque, with recorded data in red and simulated data in blue. Only the static friction parameter changes between the two model fits, which is expected due to the simplification used to calculate the normal force on each drill-string element.

A mismatch in the phase between the field and model data is seen in both examples. In Figure 15, the phase shift occurs at 50 seconds which corresponds with the initiation of axial motion of the drill-string. This motion changes the axial stress state along the drill-string and thus the frictional forces. In Figure 16, a phase shift appears at 45 seconds. In this case, the model behavior enters an increasing oscillatory pattern several cycles before the field data.

5.4. Well C: Stick dominated oscillations

The field data from **Well C** is when the well is at a larger depth and with a shallower profile – the tangent section of the well is 60° instead of the 45° as in **Well B**, which results in a higher break-off torque. This, coupled with the fact that a lower RPM i used, causes **Well C** to exhibit strong stick dominated oscillations. Downhole data was not available for this well, however, a fit of the surface data may still be made and is shown in Figure 17 and 18.

5.5. Remarks on the model comparison

Model fit is found to be very sensitive and the quality of fit varied from dataset to dataset. This is due to a number of factors:

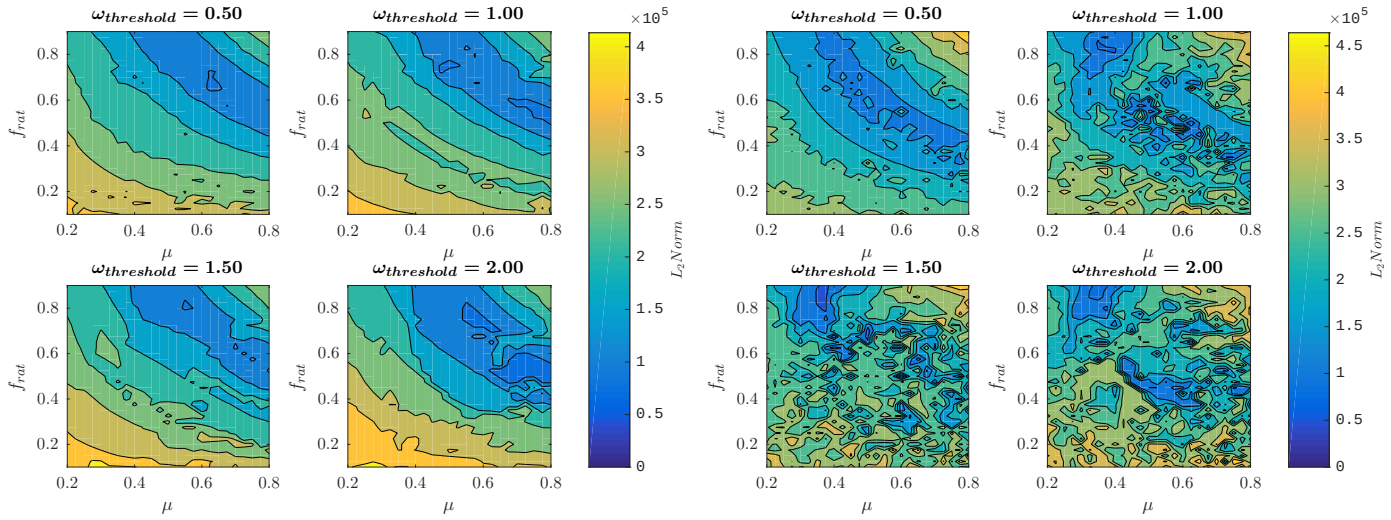

(a) Model error for a range of frictional parameters for the initial 1.5 cycles of torsional oscillations.

(b) Model error for subsequent cycles of torsional oscillations.

Figure 13: The L_2 norm of the error in fitting the model for a range of friction coefficients, μ, friction rations, f_{rat}, and angular velocity thresholds for Coulomb friction, $\omega_{threshold}$ for a depth of 1700 meters in Well B.

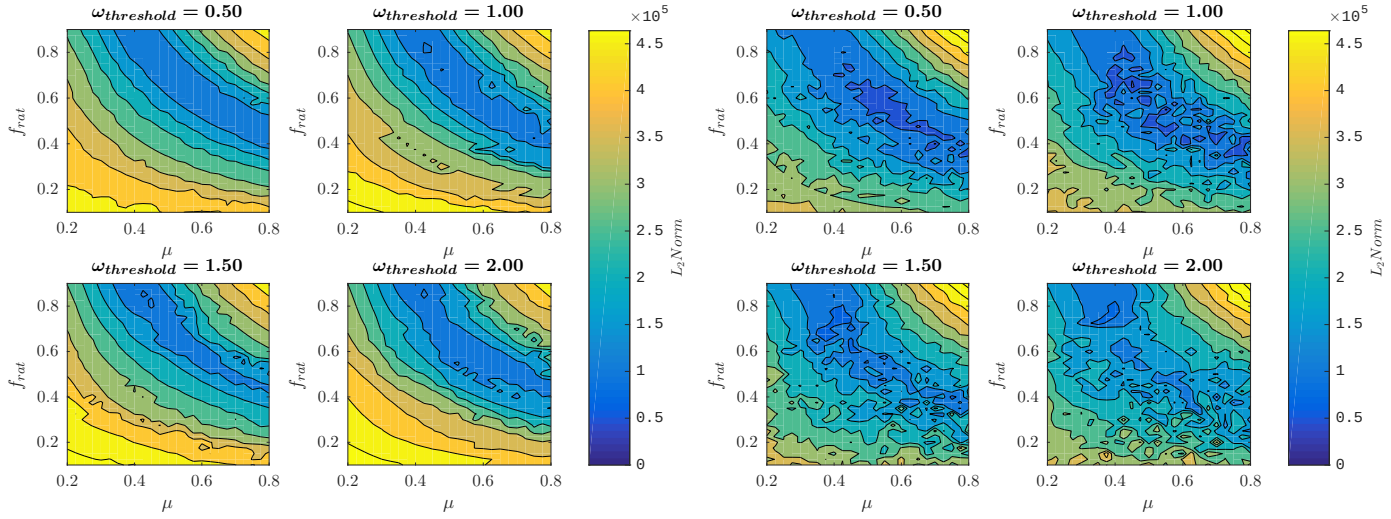

(a) Model error for a range of frictional parameters for the initial 1.5 cycles of torsional oscillations.

(b) Model error for subsequent cycles of torsional oscillations.

Figure 14: The L_2 norm of the error in fitting the model for a range of friction coefficients, μ, friction rations, f_{rat}, and angular velocity thresholds for Coulomb friction, $\omega_{threshold}$ for a depth of 2200 meters in Well B.

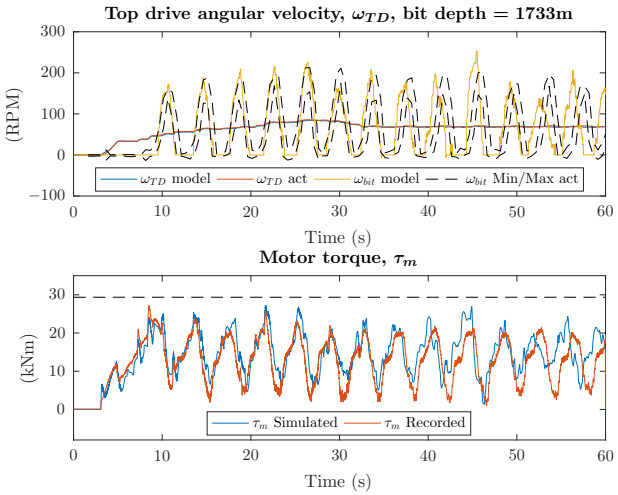

Figure 15: Recorded and simulated drill-string response at a bit depth of 1,714 m in **Well B**, using fitting parameters: $\mu_s = 0.885, \mu_d = 0.425, \omega_{Threshold} = 0.9$. Axial motion of the drillstring begins at 50 seconds.

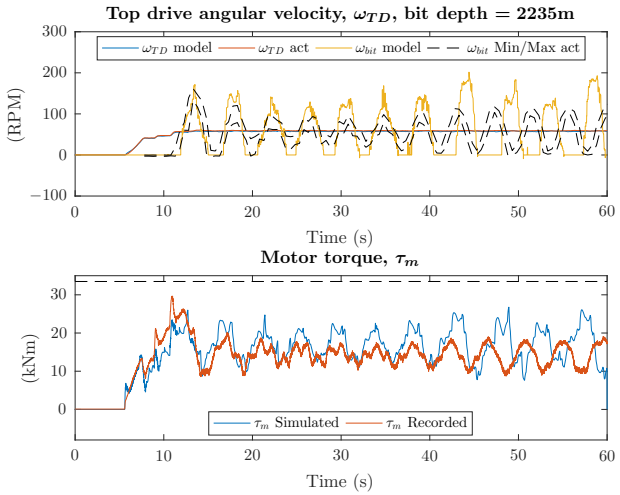

Figure 16: Recorded and simulated drill-string response at a bit depth of 2,235 m in **Well B**, using fitting parameters: $\mu_s = 0.885, \mu_d = 0.425, \omega_{Threshold} = 0.9$. No Axial motion of the drillstring is present.

- Pre-existing torsional stress state, the amount of twist existing in the drillstring, is not know at each connection event. Thus the total number of twists needed to break static friction is not know. This is very difficult to both model and quantify in field data since there is no method to to know the number of twists in the drillstring from the recorded field data.
- The model only accounts for torsional state within the drillstring and does not take into account the axial stress state. If the axial state does not change, then this is a valid assumption and only the estimate of normal force on each element is affected. However, once the drillstring begins moving axially, the model assumptions are violated and deviation between the field and simulated data appears.

A coupled axial-torsional model will improve the model fit, however, is outside the scope of this paper.

The main conclusion from the simulation study and the comparison with field data are the following:

- The model is able to qualitatively (and sometimes with high accuracy) capture the dynamics apparent in the field data.
- The model is able to recreate the qualitative differences in behavior as the Well survey and Well depths are changed. In particular it is able to capture and predict the differences of inertia and stick dominated stick-slip oscillations.
- The only tuning variables of the model is the static and dynamic Coulomb friction. The effect of changing these parameters are well defined, and crucially, we are able to achieve a high accuracy of fit to field data through tuning. This builds confidence key mechanisms of the phenomenon are adequately captured and that the model can be amenable for applications such as control and estimation of drill-string behavior [30, 31].

6. Conclusions and further work

We have presented a distributed friction model with three primarily parameters, the static and dynamic friction along the wellbore and the $\omega_{Threshold}$ of the Coulomb friction model. Using this model, we first showed the influence of the three parameters and effects on the resulting drillstring behavior. In particular we analyzed the off-bottom stick-slip limit-cycle and pin-point the how it is affected by these three key parameters, including heuristically categorizing the oscillations as inertia or stick dominated according to qualitative differences in behavior. We then applied the model to two datasets, one exhibiting inertia dominated oscillations and the second exhibiting stick dominated oscillations. The first data set included downhole data and allowed both surface and downhole response to be matched, and it was noted that model behavior diverged once axial dynamics were modified, as expected from a torsional-only model. The second data set did not include downhole data, but did exhibit strong stick dominated oscillations.

6.1. Further work

This paper isolated the effect of distributed Coulomb friction along a drillstring in a deviated wellbore and presented a model which confirms the existence of stick slip

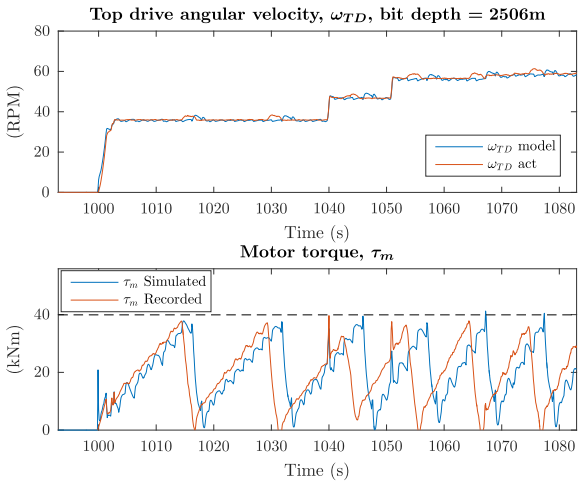

Figure 17: Recorded and simulated drill-string response at a bit depth of 2,506 m in **Well C**.

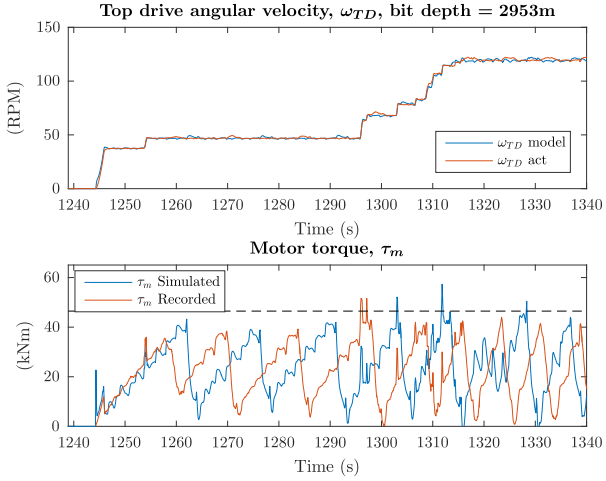

Figure 18: Recorded and simulated drill-string response at a bit depth of 2,953 m in **Well C**.

with the bit off bottom. An intuitive next step is to couple the axial and torsional dynamics to capture the behavior of the drillstring once axial motion is initiated and to add a bit-rock interaction model. This combined model may then be used in a variety of scenarios, including improved stick-slip modeling and evaluation of friction reduction techniques during slide drilling operations.

Acknowledgment

This work was supported by the Research Council of Norway, ConocoPhillips, Det norske oljeselskap, Lundin, Statoil and Wintershall through the research center DrillWell (203525/O30) at IRIS and through the Schulich School of Engineering at the University of Calgary. The authors also wish to acknowledge Shell International Exploration and Production for allowing use of their data and Sicco Dwars for his support of the effort.

Referencess

[1] J. J. Bailey, I. Finnie, An Analytical Study of Drill-String Vibration, Transactions of teh American Society of Mechanical Engineers (May 1960) (1960) 122–127.

[2] D. Dashevskiy, J. Rudat, L. Pohle, Model-Based Stability Analysis of Torsional Drillstring Oscillations, in: Proceedings of 2011 IEEE International Conferencce on Control Applications, Denver, CO, 2011.

[3] J. Brett, The Genesis of Bit-Induced Torsional Drillstring Vibrations, SPE Drilling Engineering 7 (03) (1992) 168–174.

[4] P. E. Pastusek, D. Ertas, L. Wang, J. R. Bailey, Drillstring Mechanics Model for Surveillance, Root Cause Analysis, and Mitigation of Torsional and Axial Vibrations, Proceedings of 2013 SPE / IADC Drilling Conference and Exhibition (December).

[5] M. Kapitaniak, V. Vaziri, J. Páez, K. Nandakumar, M. Wiercigroch, Unveiling complexity of drill string vibrations : Experiments and modelling, International Journal of Mechanical Sciences 101-102 (2015) 324–337.

[6] T. Richard, C. Germay, E. Detournay, Self-excited stickslip oscillations of drill bits, Comptes Rendus Mécanique 332 (8) (2004) 619–626.

[7] T. Richard, C. Germay, E. Detournay, A simplified model to explore the root cause of stickslip vibrations in drilling systems with drag bits, Journal of Sound and Vibration 305 (3) (2007) 432–456.

[8] C. Germay, N. van de Wouw, H. Nijmeijer, R. Sepulchre, Nonlinear Drillstring Dynamics Analysis, SIAM Journal on Applied Dynamical Systems 8 (2) (2009) 527–553.

[9] R. I. Leine, D. H. van Campen, W. J. G. Keultjes, Stick-slip Whirl Interaction in Drillstring Dynamics, Journal of Vibration and Acoustics 124 (2) (2002) 209.

[10] K. Nandakumar, M. Wiercigroch, Stability analysis of a state dependent delayed, coupled two DOF model of drill-string vibration, Journal of Sound and Vibration 332 (10) (2013) 2575–2592.

[11] X. Liu, N. Vlajic, X. Long, G. Meng, B. Balachandran, State-Dependent Delay Influenced Drill String Dynamics and Stability Analysis, in: Volume 7B: 9th International Conference on Multibody Systems, Nonlinear Dynamics, and Control, ASME, 2013, p. V07BT10A065.

[12] B. Besselink, T. Vromen, N. Kremers, N. van de Wouw, Analysis and Control of Stick-Slip Oscillations in Drilling Systems, IEEE Transactions on Control Systems Technology 24 (1) (2016) 226–239.

[13] Å. Kyllingstad, P. J. Nessjøen, A New Stick-Slip Prevention System, in: Proceedings of SPE/IADC Drilling Conference and Exhibition, no. March, 2009, pp. 17–19.

[14] D. J. Runia, S. Dwars, I. P. J. M. Stulemeijer, A brief history of the Shell "Soft Torque Rotary System" and some recent case studies, in: SPE/IADC Drilling Conference, Society of Petroleum Engineers, 2013, pp. 69–76.

[15] S. Dwars, Recent Advances in Soft Torque Rotary Systems, in: Proceedings of 2015 SPE/IADC Drilling Conference, no. March, London, United Kingdom, 2015, pp. 17–19.

[16] M. Yilmaz, S. Mujeeb, N. R. Dhansri, A H-infinity control approach for oil drilling processes, Procedia Computer Science 20 (2013) 134–139.

[17] T. Vromen, C.-H. Dai, N. van de Wouw, T. Oomen, P. Astrid, H. Nijmeijer, Robust output-feedback control to eliminate stick-slip oscillations in drill-string systems, in: IFAC-PapersOnLine, Vol. 48, Elsevier Ltd., 2015, pp. 266–271.

[18] E. M. Navarro-Lopez, D. Cort, D. Cortes, Sliding-mode control of a multi-DOF oilwell drillstring with stick-slip oscillations, in: Proceedings of the 2007 American Control Conference, IEEE, New York City, 2007, pp. 3837–3842.

[19] J. Brett, A. Beckett, C. Holt, D. Smith, Uses and Limitations of Drillstring Tension and Torque Models for Monitoring Hole Conditions, SPE Drilling Engineering 4 (03) (1989) 223–229.

[20] G. Halsey, A. Kyllingstad, T. Aarrestad, D. Lysne, Drillstring Vibrations: Comparison Between Theory and Experiments on a Full-Scale Research Drilling Rig, in: SPE/IADC Drilling Con-

ference, no. IADC/SPE 14760, Society of Petroleum Engineers, 1986, pp. 311–321.
[21] D. Zhao, S. Hovda, S. Sangesland, Abnormal Down Hole Pressure Variation by Axial Stick-Slip of Drillstring, Journal of Petroleum Science and Engineering In press.
[22] U. J. F. Aarsnes, O. M. Aamo, Linear stability analysis of self-excited vibrations in drilling using an infinite dimensional model, Journal of Sound and Vibration 360 (2016) 239–259.
[23] C. Germay, V. Denoël, E. Detournay, Multiple mode analysis of the self-excited vibrations of rotary drilling systems, Journal of Sound and Vibration 325 (1-2) (2009) 362–381.
[24] E. Cheng, M. A. Polak, Theoretical model for calculating pulling loads for pipes in horizontal directional drilling, Tunnelling and Underground Space Technology 22 (5-6) (2007) 633–643.
[25] L. P. Skyles, Y. A. Amiraslani, N. O. Varco, J. E. Wilhoit, D. Energy, Converting Static Friction to Kinetic Friction to Drill Further and Faster in Directional Holes, in: Proceedings of the 2012 IADC/SPE Drilling Conference, San Diego, CA, 2012, pp. 1–16.
[26] U. J. F. Aarsnes, N. van de Wouw, Dynamics of a distributed drill string : Characteristic parameters and stability maps, in preparation.
[27] S. Menand, AADE-13-FTCE-21 Borehole Tortuosity Effect on Maximum Horizontal Drilling Length Based on Advanced Buckling Modeling, in: AADE National Technical Conference and Exhibition, Oklahoma, 2013.
[28] P. Weijermans, J. Ruszka, H. Jamshidian, M. Matheson, Drilling with Rotary Steerable System Reduces Wellbore Tortuosity, in: SPE/IADC Drilling Conference, Society of Petroleum Engineers, 2001.
[29] S. Patankar, Numerical heat transfer and fluid flow, CRC press, 1980.
[30] U. J. F. Aarsnes, T. Flåtten, O. M. Aamo, Review of two-phase flow models for control and estimation, Annual Reviews in Control
[31] F. Di Meglio, U. J. F. U. Aarsnes, A distributed parameter systems view of control problems in drilling, IFAC-PapersOnLine 48 (6) (2015) 272–278.